ATLAS INTERNAL NOTE

10 August 2022

Temperature deformation tests of the ITk strip end-cap stiffening disks produced at Nikhef

Andrea García Alonso

agarciaa@cern.ch

Nikhef, Amsterdam, the Netherlands

on behalf of the ATLAS ITk collaboration

Summary

The upcoming LHC upgrade to HL-LHC sets new requirements for its detectors, and for this reason, the ATLAS experiment is preparing the ATLAS strip Inner Tracker ITk. Its End-Cap (EC) detectors are being under construction at Nikhef, in the Netherlands. The stiffening disks, made of Ultem foam with a carbon-fiber face-sheet, have been produced. They provide structural stiffness to the EC and act as a thermal barrier. To certify that the three manufactured stiffening disks comply with the specifications, the present note explains the thermal deformation tests carried out at Nikhef, at the end of 2021 and the beginning of 2022. Although it is quite difficult to measure small thermal deformations on such big structures, three tests have been performed: temperature changes, local temperature gradients, and global temperature gradients. The results show that the deformations in two disks are consistent with the specifications. The remaining disk is chosen as spare since it deforms above expected, although still mechanically acceptable.

Contents

1 Introduction

For the ATLAS upgrade, the future End-Caps (EC) of the Inner Tracker ITk strip detector [1] are being under construction at Nikhef, in Amsterdam [2]. The Nikhef ITk group has already produced the stiffening disks, that will provide stiffness to the ECs in the z direction and act as a thermal barrier. A representation of the ITk for high luminosity, as well as one of its end-caps, is shown in Fig. 1. The stiffening disk is located at the highest $|z|$, just outside the active tracking volume.

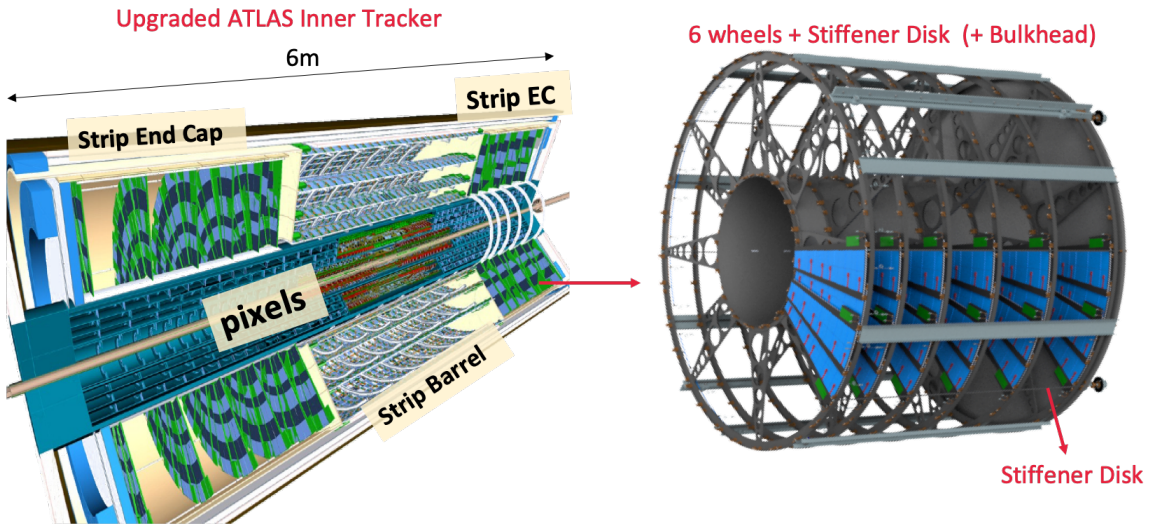

Figure 1: Upgraded ATLAS ITk on the left and one of the end-caps EC on the right. The stiffening disk is located at the highest $|z|$, just outside the active tracking volume.

Three stiffening disks have been manufactured, two will be installed in ATLAS and one spare. Each disk is two-meter diameter with a ∼74 cm diameter hole in the center (Fig. 2) at the time of these tests. At the inner radius, its thickness is 8 cm and it decreases to 3 cm at large radii, allowing for space for the services routing. Its skin is built out of carbon-fiber (CF) sheets and fire-retardant epoxy, filled with 12 kg of Ultem foam [3].

Figure 2: Stiffening disk on the aluminum support frame, during the sensors installation. This happened before moving everything into a box where the temperature was controlled.

2 Motivation

This work focuses on temperature gradients over the front and the back side of the stiffening disk that lead to unwanted out-of-plane deformations. There are three constraints that require temperature deformation tests to be performed over the stiffening disks. First of all, the necessity of operating the detector at temperatures around -25°C, requires the stiffening disk to deal with the corresponding temperature change (typically 45°C). In addition, simulations [4] predicted a temperature difference between the stiffening disk front and back surfaces, with an average gradient of ∼3°C. Finally, a temperature 'chimney effect' [4] over the stiffening disk surface will likely take place, as shown by Fig. 3.

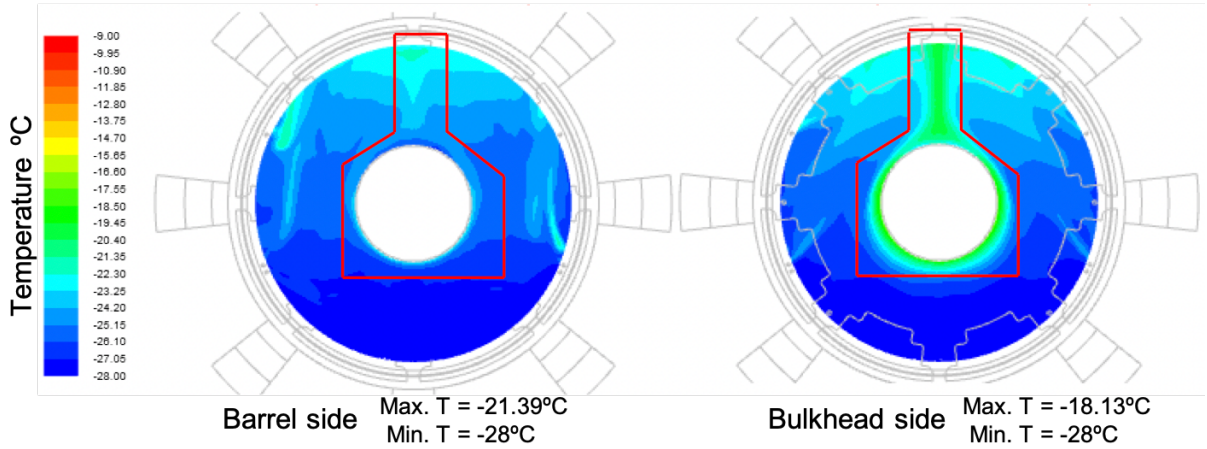

Figure 3: Temperature simulation plots showing the 'chimney effect' along the stiffening disk surface [4]. Surface in contact with the barrel on the left, and with the bulkhead on the right.

The deformation depends on structural details and features of the used materials, notably on the ratio of epoxy and CF face-sheets, whose exact value is unknown. Since Finite Element Analysis (FEA) depends on assumptions made on the amount and uniformity of these materials and at their interface with the foam core, deformations cannot be obtained from FEA. Deformations are expected of the order of hundreds of microns on the disk sagitta, based on the behaviour of a prototype disk. The sagitta is defined as the out-of-plane movement of the disk center with respect to the edge. The specifications for temperature deformations are around 300 µm for a 45°C uniform temperature change. For the gradient between disk surfaces, a 5°C average gradient was assumed during the disk design, with a maximal sagitta of 200 µm [5]. The results shown in this note must comply with these numbers, which are summarised in Table 1. Deformations up to ∼1 mm would still be mechanically acceptable, although small thermal deformations decrease the sensitivity to temperature changes and facilitate initial tracking.

Stiffening disk temperature scenario	Sagitta / µm
45°C uniform change	300
5°C gradient between surfaces	200

Table 1: Summary of the sagitta expected values (out-of-plane movements of the stiffening disk center with respect to the edge) for the temperature deformations on the stiffening disks. These numbers are defined by the specifications for the expected operating conditions [5].

3 Temperature deformation tests

To check whether the deformations comply with the specified values, at Nikhef we have tested the three stiffening disks through three tests: uniform temperature change, local gradient over the disk, and temperature gradient through the disk.

- The first test is the temperature change, where the stiffening disk shape is recorded, using LVDT sensors [6], once at room temperature, and again after uniformly rising 20°C the temperature. We conducted this test on all three disks. Additionally, for disk #3 we used a chiller to uniformly decrease the temperature by 30°C. This way, the temperature change that sets the operating conditions once installed in the detector is reproduced. We assumed that increasing the temperature leads to the exact opposite effect as decreasing the temperature.

- The second test is a local temperature gradient, achieved by placing dry ice on a region of the stiffening disk. This mimics the 'chimney effect' predicted by the simulations.

- In Section 8 we discuss the results of the most difficult test: the uniform gradient through the disk. This was achieved by heating up the box to +40°C and recording the disk deformation while opening the box. An instant temperature gradient is generated through its thickness. This test is difficult as the actual temperature gradient through the disk is not well defined, and the temperature of the supporting setup has to be kept constant.

4 Setup

Each stiffening disk was tested inside the cold box of Fig. 4, on an aluminum support frame supplied with eleven LVDT sensors [6] (pink labels in the photo). Four LVDT pairs –with their cores in contact with both stiffening disk top and bottom surfaces– are located along the outer ring, and three individual LVDTs are in contact with the top surface along the inner ring. When the pairs are represented in pictures or sketches, odd numbers refer to the top of the disk and even to the bottom.

As shown by the side view sketches of Fig.4-bottom, one surface of the stiffening disk is flat and the other one is curved, with the largest thickness at the center. Since the LVDTs are attached to the support frame, it is necessary to estimate the contribution of the support frame to the registered displacements. The contributions of the stiffening disk and the support frame will be dissociated by comparing the displacements from a temperature change with both the flat side of the disk facing up and down.

The support frame rests on the box on three points. This frame provides three support points to the stiffening disk, represented in Fig. 4 by red dots on the sketches of the stiffening disk top and side views. These support points are a set of three aluminum tubes that are replaced by another set with different height when the disk is flipped. Therefore, these two-height sets of supports introduce a systematic error, due to a different behavior with temperature. On top of this, the distribution of these points leaves the disk free enough to be subjected to global movements or tilts. Nonetheless, the sagitta calculation will remove these effects.

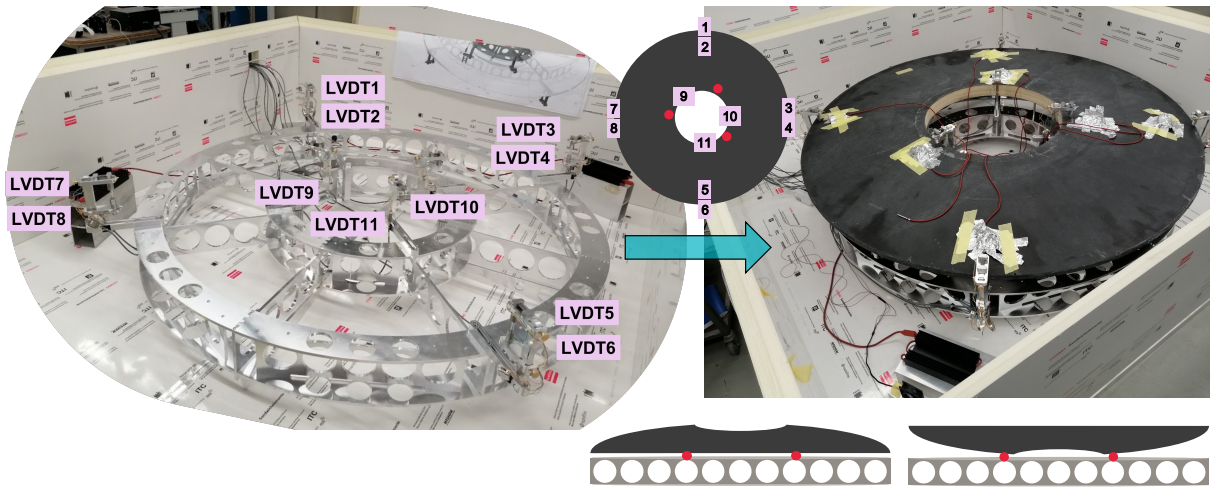

Figure 4: Left: aluminum support frame with LVDT sensors, inside the cold box. Right: same setup with the stiffening disk and temperature sensors stuck to it on both surfaces. LVDTs cores are in contact with the disk. Center: top view of the disk with the LVDTs locations. Odd numbers on the outer ring refer to top LVDTs, even to bottom ones. Red points are the lying points of the stiffening disk. Bottom: the two disk orientations: the flat side faces down and up.

Inside the cold box, heaters and fans were used for raising the temperature. A chiller with dry air was used for the cold tests on disk #3. To achieve local temperature gradients, dry ice was placed on top of the stiffening disk. Humidity and temperature sensors were also installed on both disk surfaces and other box locations. Figure 4-right shows the stiffening disk on the support frame, with the LVDTs cores in contact with its surfaces and the temperature sensors stuck to it. The next subsection describes the LVDTs calibrations.

4.1 LVDT sensors calibration

The LVDT sensor, shown in Fig. 5, is constituted by a metallic core that induces a current along the coil inside which it is placed. The sensor readout is a voltage signal over time. Movements of the core inside the coil generate voltage differences.

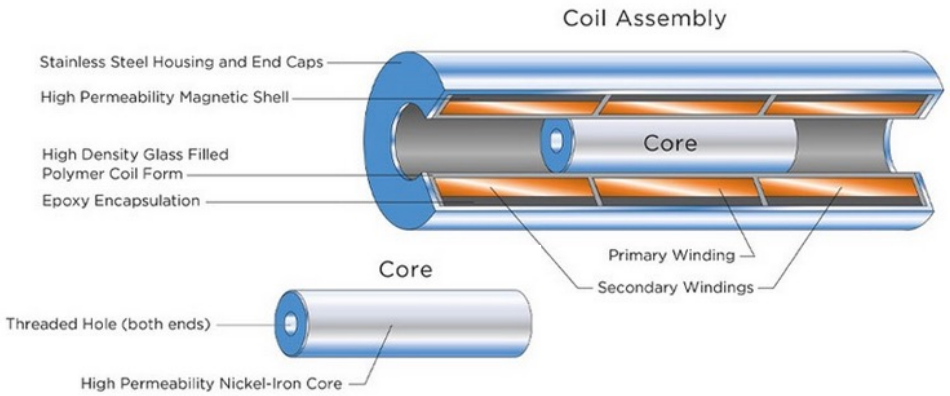

Figure 5: Representation of an LVDT sensor. The metallic core is illustrated in the center of the LVDT, position around which the voltage response is linear. Image adapted from [7].

To determine the conversion factor between the voltage difference and the correspond-

ing displacement along the coil length, each of the eleven LVDTs has been calibrated. Plots like Fig. 6, relate core positions around the coil center and the induced voltages. The slopes have been computed as the calibration factors. Although each LVDT presents its own calibration factor, in global terms, the value is 5.30±0.05 mV/µm. As shown by the residuals plot, this conversion factor is quite accurate along several millimeters.

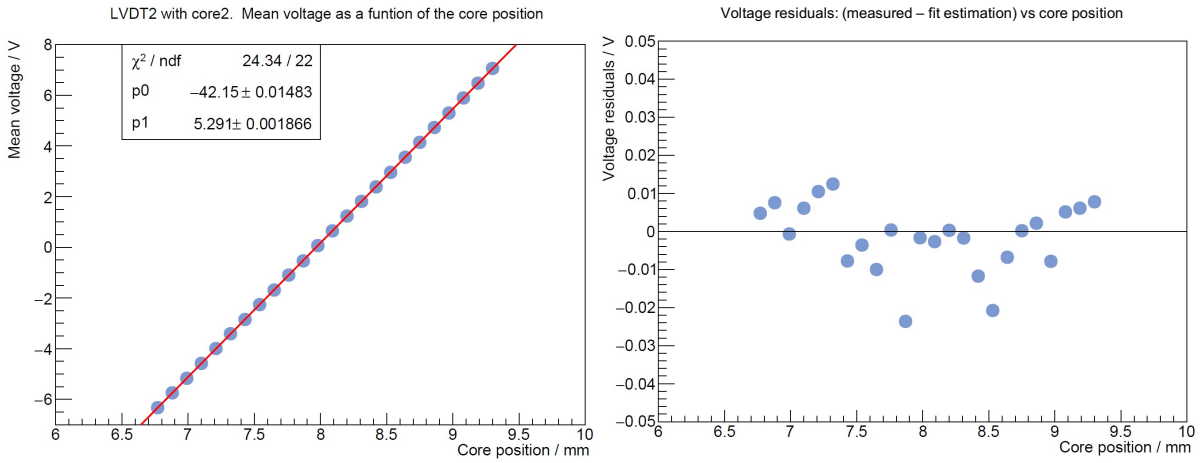

Figure 6: Calibration fit for LVDT 2 and residuals. The slope of the relation between the core position inside the coil and the induced voltage gives the LVDT calibration factor. Each point is the mean value of the voltage over one minute. Error bars (typically around ±1 mV) are shorter than the markers.

5 Data processing and reconstruction

The raw data is the voltage response of the eleven LVDT sensors over one minute at a certain temperature. Figure 7 is an example of raw data at room temperature and at +40.8°C, when the LVDTs are in contact with the stiffening disk #2. The disk flat side was facing down. The temperature values appear stable within 0.5°C.

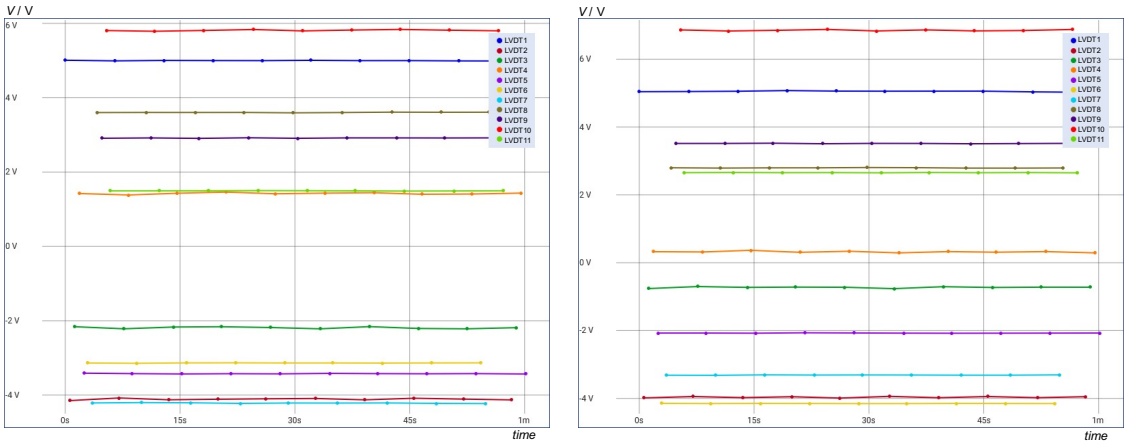

Figure 7: Raw data from the eleven LVDT sensors during one minute. Voltage readouts at room temperature T_1=21.1°C (left) and after rising the temperature to T_2=40.8°C (right). The stiffening disk under test here is the #2 lying on its flat side.

The voltage difference between room temperature and a target temperature is computed over one minute. This change is due to the LVDT cores movement together with the corresponding stiffening disk area. Figure 8 shows an example of these voltage differences, obtained from Figure 7. The values are then averaged over time and the standard deviation is computed as the statistical uncertainty.

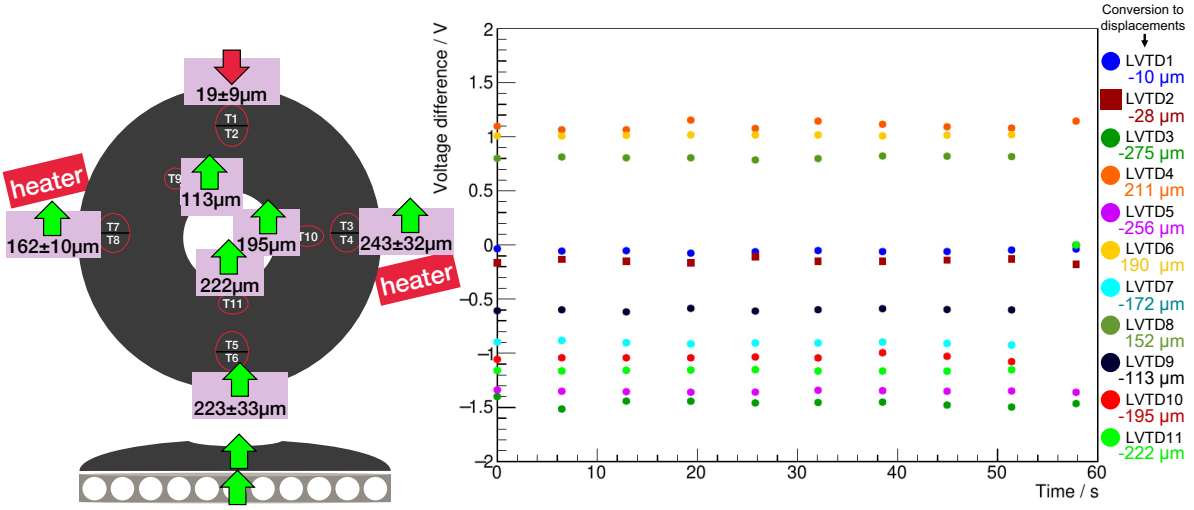

Figure 8: Voltage difference between T_1=21.1°C and T_2=40.8°C over one minute, for stiffening disk #2 with its flat side down. The legend includes the conversion to displacements of the mean voltages. The sketches (left) show the stiffening disk surface with the location of temperature sensors and LVDTs, and the side view with the support frame. Two heaters raised the temperature to 40.8°C, whose locations are represented in the sketch too. Temperature sensors are shown in red circles: when two are inside the same circle, it means they share location, each on a disk surface. Pink boxes contain displacements per LVDT at the inner circle, and per pair of LVDTs at the outer circle. Green and red arrows indicate displacement sign.

5.1 Local LVDT response

The conversion from voltage differences to displacements is obtained with the calibration factor of each LVDT, which gives a conversion of roughly 200 µm per volt. The legend of the plot in Fig. 8 includes the converted values from each LVDT, with an associated uncertainty of 6 µm, obtained by error propagation from the statistical uncertainty and the one of the calibration factor.

The sketch of Fig. 8 shows the front and side views for this measurement. The front view displays the location of the heaters and the temperature sensors. The displacements recorded by each LVDT are shown at the corresponding location. Those LVDTs installed in pairs along the stiffening disk's outer ring –one on top and one on bottom– are matched to get an average value at that point. The uncertainty of those values is given by the standard deviation between the two measurements, typically around 13 µm, that propagates through the calculation.

The example of Fig. 8 also shows displacements at the inner LVDTs, close to where the disk is supported. Correlated effects are expected from the thermal expansion of the Ultem foam core of the disk (∼50 µm/m/K) and the aluminum support of the LVDTs. However, the results also show that the three disk supports do not behave similar. We

attribute this to mechanical imperfections of the support interfaces in combination with the thermal expansion of the disk. These supports may also move and expand with respect to the LVDT supports. Therefore the disk is subjected to global movements (tilts) during the tests. To extract the deformation of the disk we use the sagitta calculation, which is independent to these global effects.

5.2 Global movement and deformation

The registered movements caused by the temperature change include the deformation of the aluminum support frame on which the stiffening disk is placed. To measure its contribution and obtain the movements exclusively due to the stiffening disk, we flip the stiffening disk along the axis defined by LVDTs 1 and 5 (see Fig. 9), and we repeat the temperature test. When the stiffening disk flat side faces down, both the disk and the setup contribute upward when rising the temperature, as indicated by results like Fig. 8. However, after flipping the disk, its effect changes sign. Consequently, by subtracting the displacements obtained at each orientation, as represented in Fig. 9, the setup contribution disappears, and the result divided by two gives the movements due to the disk change with temperature. On the other hand, by summing up, the contribution of the setup is obtained, value found to be around 100 µm of global movement.

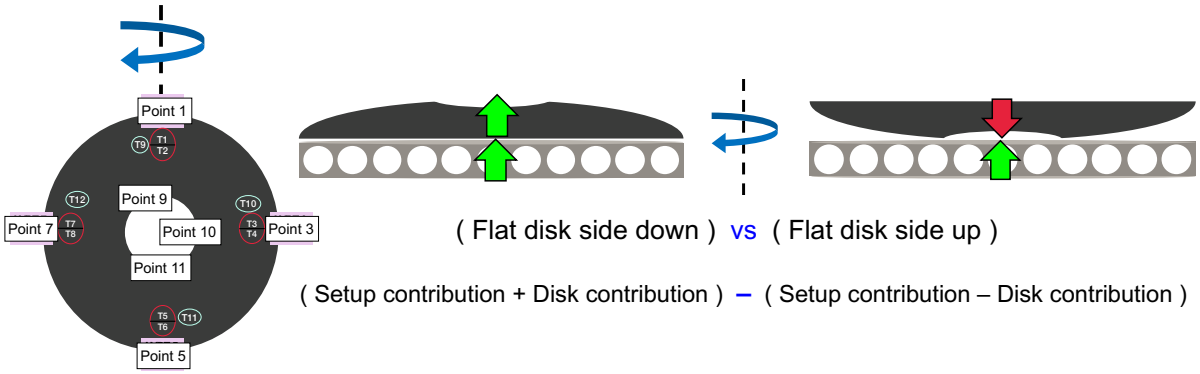

Figure 9: Sketches of the two considered orientations of the stiffening disk on the support frame. When the flat side faces down both the disk and the setup contributions to the movements add up. When the flat side faces up, the contributions counteract. The disk is flipped along the axis defined by points 1 to 5.

Disk orientations comparison is the only method to dissociate the contribution of the disk and the setup, but it assumes symmetric global movements with respect to the center. This means that, along one disk diameter, the deformation is assumed to be mirror-symmetric with respect to its center, like a bow shape. If asymmetric movements existed, like an s-shape, bigger global movements than the actual values could be obtained.

For each disk orientation, the displacements of the three inner ring LVDTs are averaged into a single value, representative of the central disk region. The mean value of the displacements registered by each LVDTs pair along the outer ring represents the displacement at each of those border points. The standard deviations are computed as the associated errors.

5.3 Reconstruction of the sagitta

The sagitta calculation translates the global movements (based on the local displacements registered by the LVDTs) into absolute deformations. The sagitta calculation is not affected by tilts due to small instabilities from the three disk supports. Two axes —from Point 1 to 5 and from Point 3 to 7 in Fig. 9— over each stiffening disk are considered. First, the two sagittas are computed for each disk orientation, like in Fig. 10, where one of the four sagittas is represented in green. Through these plots, the deformation of the disk together with the setup is obtained.

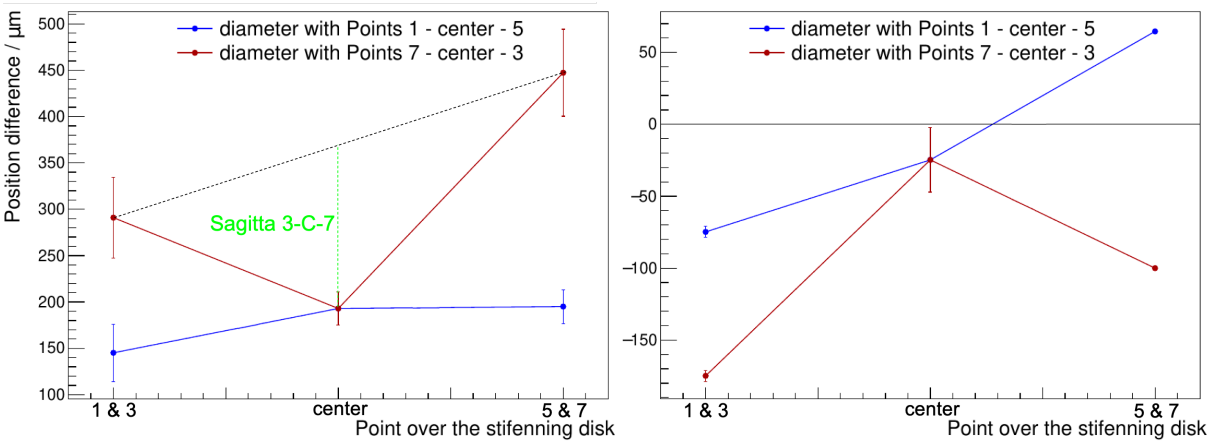

Figure 10: Disk displacements along two axes over the stiffening disk #3, at each orientation (left: flat side down, right: flat side up). From Fig. 9, Points 1 to 5 define the axis in blue and Points 7 to 3 the one in red, whose X-axis is horizontally flipped for plotting purposes. The central value is the mean of the three inner LVDTs. For each axis, the sagittas are calculated like sag 3-C-7, drawn in green as an example on the left plot. The black dotted line is drawn to connect the disk extreme points of that axis.

5.4 Disentangle the disk and setup deformations

To obtain the actual disk deformation, the sagittas from the axis 1-C-5 and 1-C-7 are recalculated after computing the half of the difference between the displacements at the two orientations, as previously explained in Section 5.2.

Plots like Fig. 11 are obtained, with just the stiffening disks deformation. They are obtained from the displacements computed for the sagittas calculation of Fig. 10. The position difference between the two orientations displacements at each point along the axes is plotted here. The corresponding uncertainty of these differences is obtained through error propagation.

The sagittas calculations, which for this last plot represents the actual disk deformation, are performed by fitting the two values of the two displacements at each axis extreme (which in the last plot represents the disk deformation at those points) and computing the difference between this fit and the data at the center (as represented by the green line in Fig. 11).

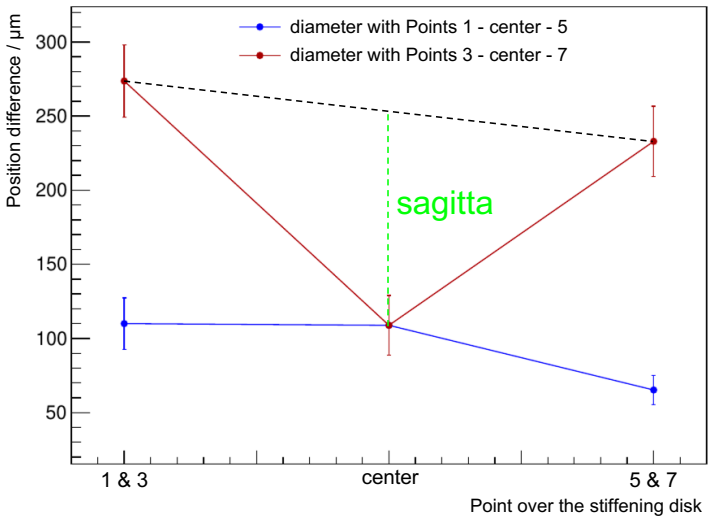

Figure 11: Disk displacements along two axes over stiffening disk #3, removing the setup contribution. From Fig. 9, Points 1-5 define the axis in blue and Points 3-7 the red one. Black dotted line connects the disk extreme points of one axis. In green: the sagitta for that axis. The displacements at the axes extremes are the half of the difference between the mean of the two LVDTs at each orientation. The displacement at the disk center is the half difference between the mean of the three inner LVDTs at each orientation. The error bars are the standard deviations.

6 Results for a temperature change

In this and the two following sections, the results of the three thermal tests we have carried out are presented. These results were obtained with the data processing of Section 5.

The present section shows the results of the temperature changes. For each stiffening disk, the +20°C temperature change was performed using two heaters. The recorded global movements are shown in Fig. 12 top row and bottom left. For stiffening disk #3, the -30°C temperature change was performed too, and the disk #3 data is shown on the bottom right of the same figure.

Figure 12 shows global movements in all the setups. The top left part of Fig. 12 shows the +20°C temperature change for stiffening disk #1 in each orientation, where the largest registered movement is 453 µm when the flat side faced down. The top right part shows stiffening disk #2 responses, for which the recorded maximum value is shorter: 243 µm, for the same orientation. The bottom left part, with disk #3, presents a maximum of 447 µm, with the flat side facing down. All these numbers include the setup contribution, which is corrected in later plots by subtracting the measured global movements at the two disk orientations.

Regarding the shape of the change, stiffening disks #2 and #3 exhibit more similar displacements than disk #1. It could be a consequence of more resembling manufacturing processes for the two last disks, where the amount of epoxy in the face sheets was better controlled than for disk #1.

It can also be observed that the disks do not present rotational symmetry: they seem to deform in the shape of a 'pringle', thus with the out-of-plane deformation in opposite directions along the two axes. However, since these values are highly affected by the setup and the presence of tilts, final conclusions cannot be drawn without further analysis, which we discuss below.

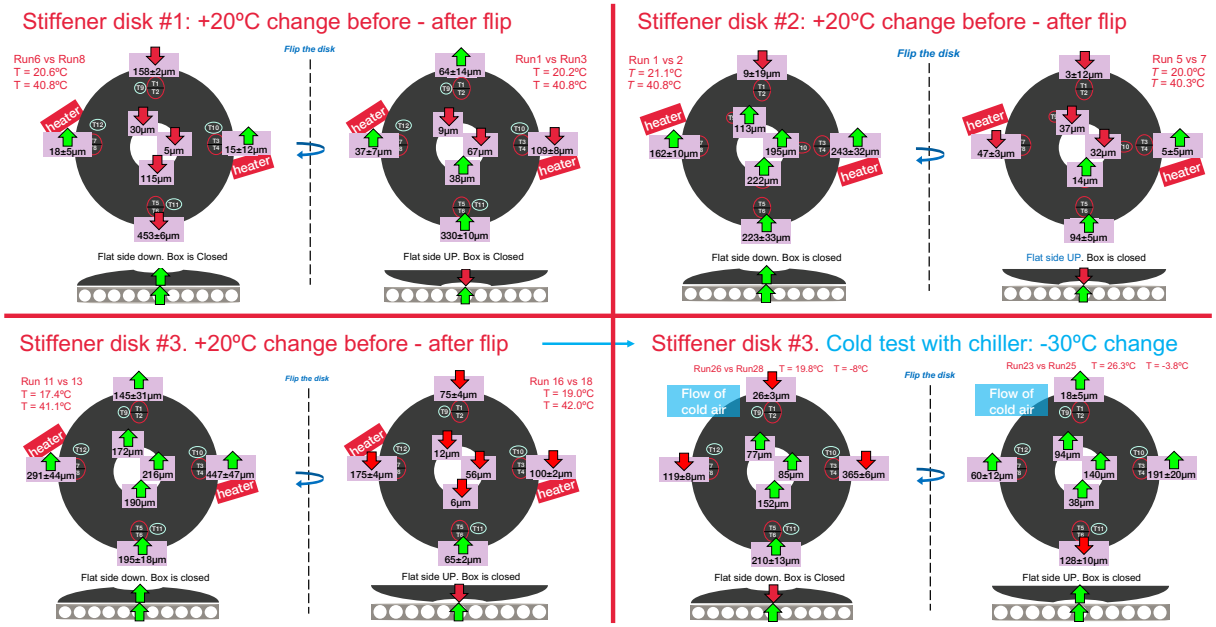

Figure 12: Global movements at flat-side up and down orientations, as indicated by the bottom sketches for each measurement. Red titles for +20°C temperature change on all the stiffening disks and blue for -30°C change on stiffening disk #3. These displacements contain the combined contribution of the disks and the testing setup (support frame and the other aluminum supports), as well as any possible disk tilt. Arrows indicate the sign of the movements at single inner LVDTs and pairs of outer ring LVDTs.

For disks #2 and #3, the LVDTs at the inner ring register similar effects for a +20°C temperature change, while disk #1 appears to behave somewhat differently.

6.1 Sagitta per disk orientation

A first analysis is done by calculating the sagittas, as described in Section 5.3, for the cases considered in Fig. 12. Figure 13 shows the global movements over the two axes at each stiffening disk and orientation. The first axis, in blue, is defined by LVDTs 1 and 5 in the central sketch of Fig. 4. The second axis, in red, is the one that connects LVDTs 3 and 7. The extremes of this second axis are exchanged, making it possible to plot together in one dimension the two axes and the individual readouts of the inner LVDTs.

6.1.1 Global tilt of the disk

In Fig. 13, the value at the disk center is computed as the averaged displacement of the three inner LVDTs. To check the reliability of this number, the individual measurements of these LVDTs are represented by the three crosses. The readout from LVDT 11 is included with a blue cross, since it belongs to the blue axis. The readout from LVDT 10 is shown with a red cross, because it belongs to the axis defined by LVDTs 7 and 3.

The green cross represents LVDT 9, which does not belong to any of the considered axes but, located on the other side, it helps to identify disk tilts. Any tilt will be observed from the deviation of the individual three values. All these values, extracted from Fig. 12, contain the deformations of the stiffening disks together with the contribution of the setup.

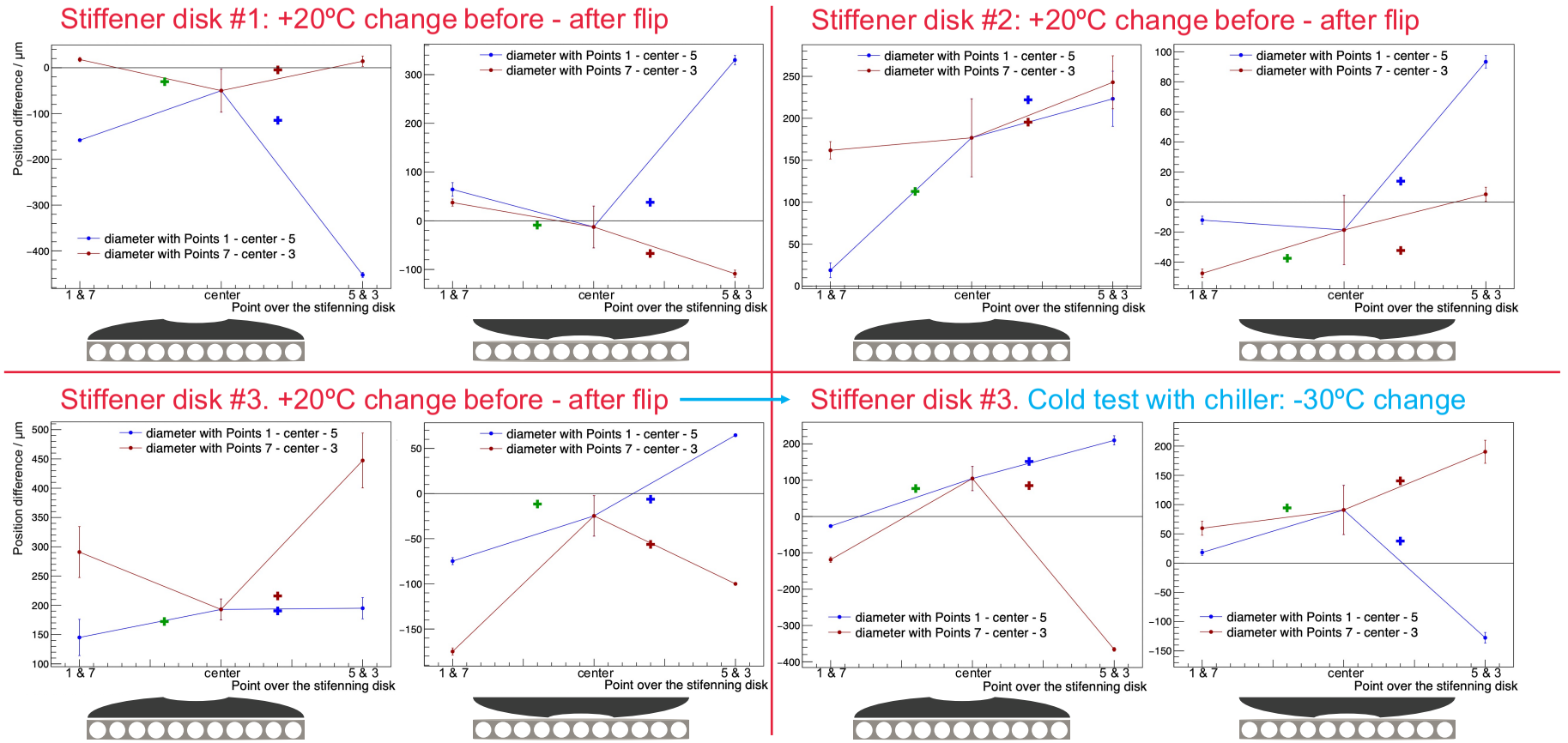

Figure 13: Displacements along two axes over the three stiffening disks for both orientations. Setup contribution is still included in these values. These plots were created with the data of Fig. 12. Points 1 to 5 from Fig. 9 define the axis in blue, while Points 3 to 7 define the axis represented in red, whose X-axis is horizontally flipped for plotting purposes. The global displacement at the center is the mean value of the three inner LVDTs, however, the displacements of the inner LVDTs are also included for double-checking possible tilts. To compare with the axis in blue, the displacement of LVDT 11 is included with a blue cross. For the red axis, the LVDT 10 is shown in red. LVDT 9 is added in green since it does not belong to any of the axes. A black horizontal line is displayed to indicate null displacement. The resulting sagittas are computed in Table 2.

In each plot, the dispersion between the three crosses gives an idea of the disk tilt. While disk #3 with the flat side down at the +20°C temperature change seems to be close to horizontal, disk #2 in the same configuration is tilted more than 100 µm. As a consequence, the larger the tilt, the less reliable the estimation of the central value is.

6.1.2 Shape of the deformation

When comparing the lines with their crosses, the match is evident for short sagittas (<50 µm). For larger sagittas, there is a deviation with respect to the straight line, as expected for a bow shape. This agreement confirms the direction of the deformation is symmetric with respect to the center, for each axis: the deformation is consistent with a bow shape and not with an s-shape.

For both disk orientations, the shape of the global deformation seems the same, as expected. The disk contribution is dominant and it is just inverted when changing the orientation. Quantitative differences are due to the setup contribution and tilts.

The sagitta values for the up and down orientations at several temperature changes are shown in Table 2, corresponding to the plots in Fig. 13. Remind that the sagitta is not affected by global tilts of the disk, but the deformations of the setup itself are still present. These values show great consistency before and after flipping the disk. Along both axes, the negative temperature change performed on disk #3 manifests a setup contribution which may be due to the chiller-element, which was installed close to LVDTs 7&8. The chiller performs unpredictable thermostatic on/off cycles, which can have different effects on the disk than on the aluminum setup, as different time constants are involved.

stiffening disk	temperature change	Flat side	1-C-5 sag / µm	3-C-7 sag / µm
#1	+20°C	down	-255 ±51	66 ±55
#2	+20°C	down	-56 ±67	26 ±67
#3	+20°C	down	-23 ±42	176 ±63
#3	-30°C	up	-145 ±49	34 ±58
#1	+20°C	up	210 ±55	-23 ±50
#2	+20°C	up	59 ±26	-3 ±27
#3	+20°C	up	20 ±25	-113 ±25
#3	-30°C	down	-13 ±41	-347 ±40

Table 2: Sagittas at the two considered axes (points 1-center-5 and 3-center-7) over each stiffening disk, temperature change, and orientation. The positive temperature changes with the flat side down are compared on the top part, together with the negative change with the flat side up. The rest of the tests are compared on the bottom part. These values were obtained from Fig. 13 and contain the support frame contribution to the displacements.

6.2 Deformation corrected for the support frame contribution

The second part of the analysis consists of plotting the difference in displacements between the disk orientations, as described in Section 5.4, to remove the setup contribution and get the disk deformation. The fits in Fig. 14 show the actual deformation along the two axes of the stiffening disks, calculated with Fig. 12. Like the sketch on the bottom, the flat side should be considered facing down, so positive deformations in these plots mean

upward movements with respect to that. In all the disks, there is a considerable different deformation between the two axes. Here again, the stiffening disk #1 presents the largest deformations.

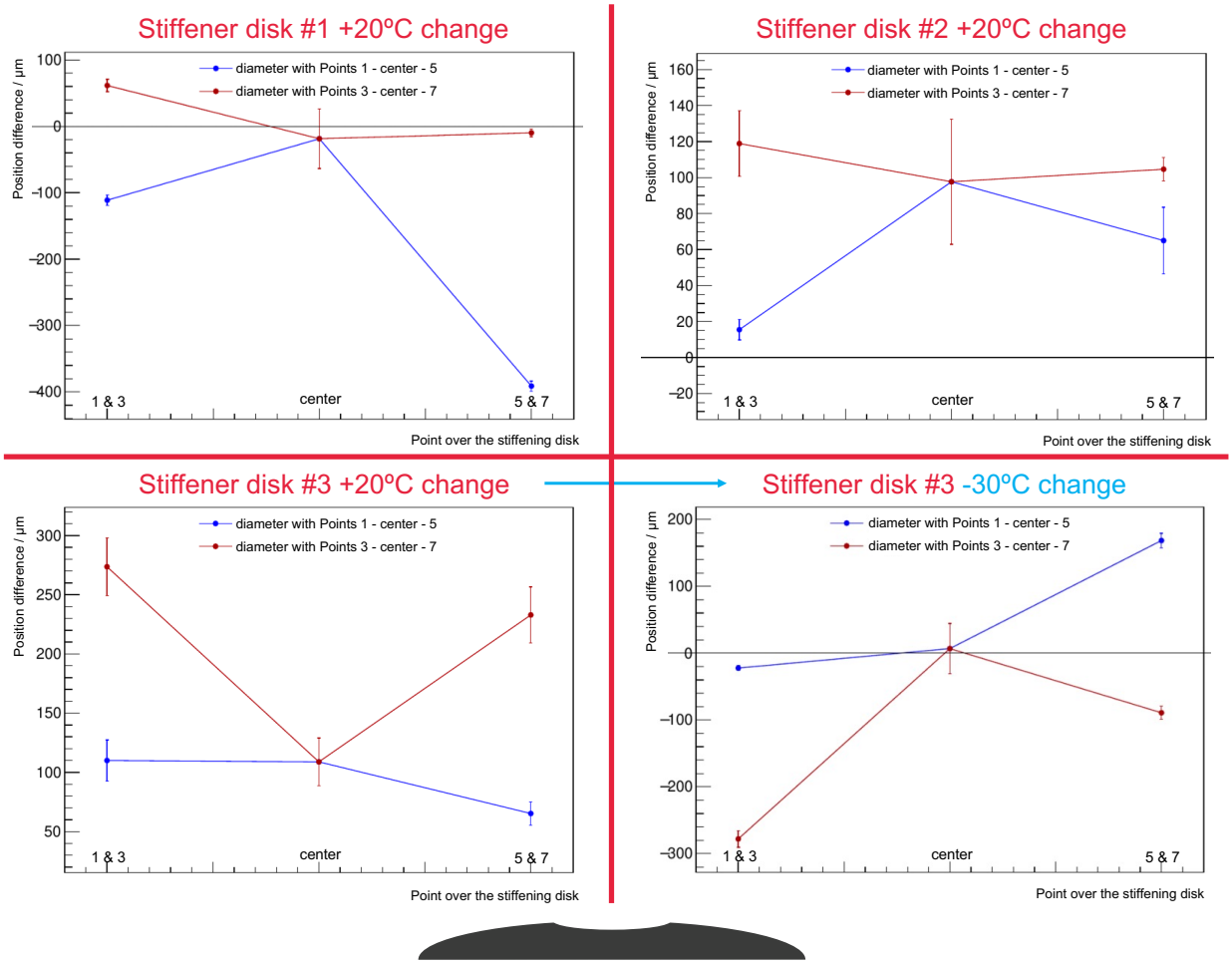

Figure 14: Displacements at the points considered in the sketch of Fig. 9 over the stiffening disk, at the same four situations of Fig. 12. Setup contributions were removed subtracting the displacements from both disk orientations. The sign of the displacements should be considered over the flat side down orientation, like in the bottom sketch. These plots provide the information to extract the numbers of the disks deformation, shown in Table 3.

In the three disks, it seems that perpendicular axes deform in opposite directions: when the curvature of one is positive, the other one is negative. Moreover, when one is close to flat the other one gets its maximum curvature. No examples of both getting largely deformed at the same time have been found. This means that the disks deform in the shape of a 'pringle', and not as a bowl, confirming the preliminary conclusion above.

The stiffening disk #3 plots, at the bottom row, consider the same axes over the same disk, therefore these fits can be quantitatively compared. Although the temperature changes differ 10°C, the direction and value of the deformations are compatible between the two tests, taking into account that the sign of the deformations is opposite.

The sagittas are computed from these plots and they are displayed in the first four rows of Table 3. The largest computed deformation (disk sagitta) is 233 µm, at the axis in blue of stiffening disk #1, for a 20°C temperature change. When extrapolated to a 45°C change,

this sagitta amounts to around 524±50 µm. Although the uncertainty is relatively large, disk #1 deforms more than expected. On the other hand, the deformations registered in the other disks do not exceed the 285 µm for this 45°C change (registered by stiffening disk #3 when tested with the chiller). Consequently, these tests show deformations in stiffening disks #2 and #3 that largely comply with the specifications.

7 Results for a local temperature gradient

In order to reproduce the 'chimney effect' predicted by the simulations, some dry ice was placed on a region of the top surface of the stiffening disk #2, as shown in Fig. 15. The disk was originally at room temperature and it stayed inside the open box. The stiffening disk #3 was tested in the same way too, registering shorter global movements. As a consequence, the stiffening disk #2 results are discussed here, to consider a worse case scenario.

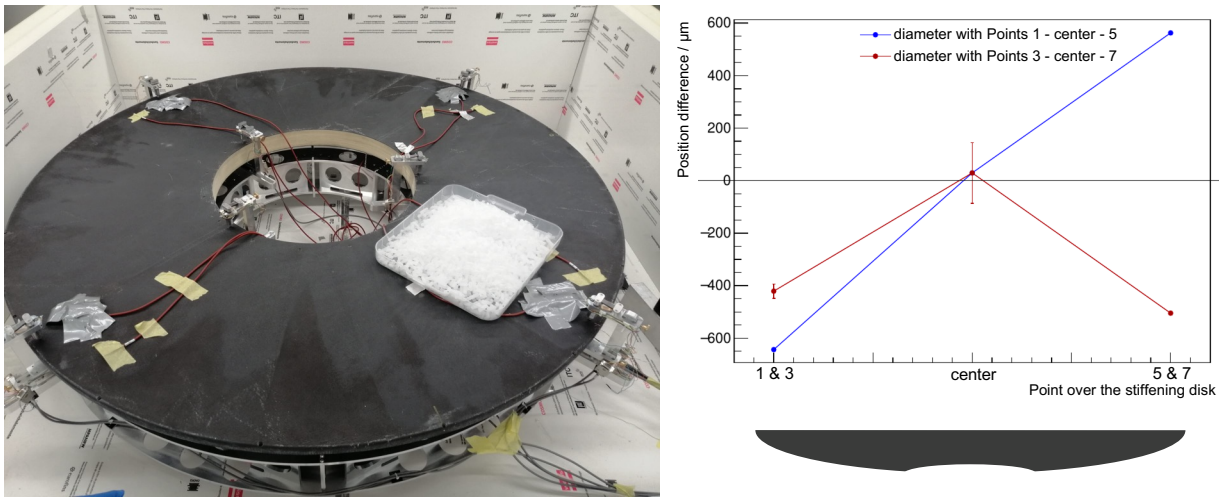

Figure 15: Dry ice test on stiffening disk #2. Left: setup with the dry ice on the top surface of the disk, close to the LVDT 1. Cold box remained open during the test. Original temperature was room temperature. Right: registered global movements along the two disk axes for calculating the sagittas. Only the flat side up configuration is considered, as represented by the bottom sketch.

In the area close to it, the dry ice dropped the temperature to -15°C on top of the disk and +16°C at the bottom. This constitutes a vertical local gradient of 30°C across the disk thickness. Since the box stayed open, the rest of the disk remained at room temperature. As a consequence, there was a gradient over the disk of 36°C: from -15°C close to the dry ice to +21°C far from it.

The data processing explained in Section 5 leads to the plot in Fig. 15, to obtain the sagittas at the two considered axes. In this test, just one stiffening disk orientation is studied, because there is no setup deformation to be removed, since the dry ice is not in contact with it, it should remain unaffected.

From this test, the obtained sagittas were 80±85 µm and 495±85 µm with this combination of local 30°C gradient through the thickness and 36°C gradient over the surface. Converted to deformations per 5°C, these values are 13±14 µm and 83±14 µm. This is

once again in agreement with the expected deformation, which was around 200 µm for a 5°C gradient between surfaces.

8 Results for a global temperature gradient

Although a global gradient is something difficult to test, a temperature gradient was achieved by heating up to +40°C the box with the stiffening disk #1, and recording the LVDTs readouts while opening the box and waiting for room temperature. The stiffening disk flat side was facing down. The temperature sensors were isolated from the surrounding air, except sensor T12, whose behavior clearly differs from the rest in Fig. 16.

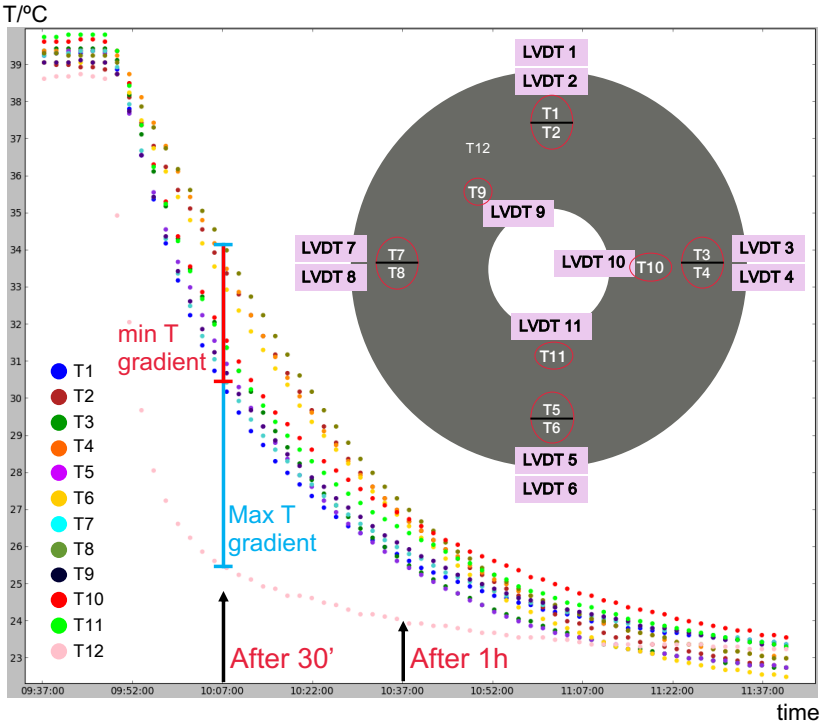

Figure 16: Temperature sensors readout after opening the box previously heated up at +40°C. All sensors were isolated, except T12. Their locations are shown in the sketch. Stiffening disk #1 flat side was facing down. At the moment when the largest gradient is achieved —30 minutes after the start of the data taking— two temperature gradients are considered: a minimum one of 3.5°C and a maximum one of 9°C.

A top-bottom surface temperature gradient is achieved, although its exact value is unknown. To make an estimation, we take the extreme values of the temperature gradient at the moment when the largest temperature difference is obtained, 30 minutes after the start of the data taking. The first extreme is the 9°C difference between the non-isolated temperature sensor on top and one isolated sensor on bottom. The other extreme is the 3.5°C difference between an isolated top sensor and an also isolated bottom sensor.

To calculate the displacements, the LVDTs readouts after 30 minutes are compared with the readouts after 1 h. This second readout is the reference, because the temperature sensors response gets uniform then.

Due to the complexity of this test, there is no sagitta calculation, therefore just one disk orientation is considered for this estimation.

The largest global displacement between the two readouts is 245±2 µm at LVDTs 1&2, for this 6±3°C gradient. Considering the maximum temperature gradient, this corresponds to 135 µm per 5°C, and considering the minimum temperature gradient, it is 350 µm per 5°C. From these numbers, it can be safe to conclude an average number of 243±100 µm per 5°C, which complies with the specifications that expected numbers around 200 µm for a 5°C gradient.

9 Comparison of the results with the specifications

Table 3 summarises the main results from the three tests performed. The first four rows show the deformations (sagittas) of the disks for the two considered axis, based on Fig. 14. The corresponding extrapolation to a temperature change of 45°C is given, for comparison with the specifications.

Stiffening disk	Type of test	deformation at 1-C-5		deformation at 3-C-7	
		measured	for 45°C	measured	for 45°C
#1	+20°C change	233 µm	524 µm	45 µm	101 µm
#2	+20°C change	57 µm	128 µm	14 µm	32 µm
#3	+20°C change	21 µm	47 µm	144 µm	324 µm
#3	-30°C change	66 µm	99 µm	190 µm	285 µm
#2	local gradient & surface gradient	13±14 µm / 5°C		83±14 µm / 5°C	
#1	global gradient through disk	243±100 µm / 5°C			

Table 3: Stiffening disk deformations (sagittas) at two perpendicular axes (defined by points 1-center-5 and 3-center-7 on Fig. 9) during the thermal tests. The deformation at each temperature change test is shown under 'measured', while their extrapolations to a 45°C change, as the one given by the specifications, are shown on their right. The largest global movement registered for the global gradient test is shown on the last row. When not specified on the table, the uncertainty is ±50 µm. The specifications set the expected values of the temperature expansion around 300 µm for a 45°C uniform temperature change. For gradients, deformations are expected around 200 µm for a 5°C gradient between surfaces.

As these values show, the stiffening disks #2 and #3 comply with the specifications, which were 300 µm for a 45°C uniform temperature change. Since disk #1 presents results slightly larger than this, with a 524 µm sagitta, it is decided to keep it as spare. Nonetheless, this disk would still be useful, because the magnitude of its deformation does not entail a problem. The other two disks behave as expected. One could argue that we measure 'only' two axis and have not seen the maximum deformation of the 'pringle' shape. In the worst case, assuming a harmonic behaviour, an additional $sqrt(2)$ factor could be applied to the deformations. Within the uncertainties, notably for disk #2 and #3, the deformation would still comply with the expected (or targeted) values. Note that these results have an uncertainty of 50 µm, obtained from the error propagation of all the systematic uncertainties previously mentioned.

The last two rows of Table 3 show the results obtained in the two temperature gradient tests. These results indicate that the disk deformations due to temperature gradients are consistent with the expected specification of 200 µm for a 5°C gradient between surfaces.

10 Conclusions

The present note summarises the work done at Nikhef to test the thermal deformations of the three stiffening disks that have been manufactured for the future ATLAS ITk End-caps. Although it is difficult to measure small thermal deformations on such a big structure, we managed to perform three types of tests: temperature change, local temperature gradient, and global temperature gradient. Global displacements at several points along the disks have been recorded for each test. The disks were placed with the flat surface looking up and down, to estimate and eliminate the contribution of the setup to the measured displacements affected by the support frame and other aluminum structures. Two perpendicular axes over the disks have been chosen to calculate the values of their sagittas, correcting for disk tilts during data taking. The results have been compared with the expected values and it is concluded that all the measured deformations are consistent with the specifications, as summarised by Table 3. It has been shown that the results of stiffening disks #2 and #3 are consistent, while stiffening disk #1 is slightly off. This disk presents larger deformations with temperature, therefore it is chosen as spare.

References

[1] Technical Design Report for the ATLAS Inner Tracker Strip Detector. Technical report, CERN, Geneva, Apr 2017. Available at https://cds.cern.ch/record/2257755.

[2] Nationaal instituut voor subatomaire fysica: Nikhef. https://www.nikhef.nl.

[3] Marcel Vreeswijk. Epoxies and Plastics in the ITk –safety issues–, 2019. Available at https://indico.cern.ch/event/857146/contributions/3607931/attachments/1928760/3200679/Strip_materials.pdf.

[4] Pedro Mafa. ITk Humidity and Temperature Modelling, 2021. Available at https://indico.cern.ch/event/998507/.

[5] Marcel Vreeswijk. Strip End-cap PRR, Dec 2019.

[6] HR Series general purpose LVDT sensors. Specifications available at https://www.te.com/usa-en/product-CAT-LVDT0020.html?q=lvdt&n=486604&type=products&samples=N&inStoreWithoutPL=false&instock=N.

[7] Linear Variable Differential Trans-former. https://www.te.com/usa-en/industries/sensor-solutions/insights/lvdt-tutorial.html#chapter-2-dl, [Accessed: 2022.04.07].